45th AIAA/ASME/ASCE/AHS/ASC Structures, Structural Dynamics & Materials Conference and 12th AIAA/ASME/AHS Adaptive Structures Forum, Palm Springs, CA, 19-22 Apr. 2004, paper # AIAA-2004-1983

Embedded Ultrasonic Structural Radar with Piezoelectric Wafer Active Sensors for Damage Detection in Cylindrical Shell Structures

Victor Giurgiutiu* and Lingyu Yu†
University of South Carolina, Columbia, SC 29208, *victorg@sc.edu*

2-Lt. Dustin Thomas‡
Air Force Research Laboratory, WPAFB, OH 45433

Structural health monitoring (SHM) is a major component of the vehicle health monitoring (VHM) concept currently considered for the civilian and military aerospace applications. Piezoelectric wafer active sensors (PWAS) are one of the candidate embedded sensors considered for SHM applications. PWAS are inexpensive, non-intrusive, un-obtrusive, devices that can be used in both active and passive modes. In active mode, PWAS generated Lamb waves that can be used for damage detection through pulse-echo or pitch-catch techniques. An efficient application of the pulse-echo method with PWAS technology is through the phased array technique. In the embedded ultrasonics structural radar (EUSR) concept, an array of closely spaced PWAS is used to detect structural cracks based on the scanning beam principle with guided Lamb waves. A scanning beam of ultrasonic Lamb waves works like "structural radar". When encountering a crack, it generates echoes and backscatter. This concept was initially developed by the authors for guided Lamb waves traveling in flat plates. In this paper, the EUSR concept is extended to cylindrical shells. First, the theory of guided waves in cylindrical shells, with the associated modes and dispersive frequencies is reviewed. It is shown that cylindrical shells accept three types of guided ultrasonic waves: longitudinal, flexural, and torsional. The first and second of these ways can be associated with the Lamb waves in flat plates, while the third can be related to the shear-horizontal guided waves in flat plates. Subsequently, the paper describes validation experiments performed on cylindrical shells of various curvatures. It is shown that the EUSR concept works on cylindrical shells with curvatures representative to actual aircraft structure just as well as it works on flat plates.

I. Introduction

Embedded nondestructive evaluation (NDE) is an emerging technology that will allow the transition of the conventional ultrasonics methods to embedded structural health monitoring (SHM) systems such as those envisioned for vehicle health management (VHM). SHM for VHM requires the development of small, lightweight, inexpensive, unobtrusive, minimally invasive sensors to be embedded in the airframe with minimum weight penalty and at affordable costs. Such sensors should be able to scan the structure and identify the presence of defects and incipient damage. Current ultrasonic inspection of thin wall structures (e.g., aircraft shells, storage tanks, large pipes, etc.) is a time consuming operation that requires meticulous through-the-thickness C-scans over large areas. One method to increase the efficiency of thin-wall structures inspection is to utilize guided waves (e.g., Lamb waves) instead of the conventional pressure waves. Guided waves propagate along the mid-surface of thin-wall plates and shallow shells. They can travel at relatively large distances with very little amplitude loss and offer the advantage of large-area coverage with a minimum of installed sensors. Guided Lamb waves have opened new opportunities for cost-effective detection of damage in aircraft structures, and a large number of papers have recently been published on this subject. Traditionally, guided waves have been generated by impinging the plate obliquely with a tone-burst from a relatively large ultrasonic transducer. Snell's law ensures mode conversion at the interface, hence a combination of pressure and shear waves are simultaneously generated into the thin plate. However, conventional Lamb-wave probes (wedge

* Associate Professor, Department of Mechanical Engineering, Univ. of South Carolina, 300 S. Main St., Columbia, SC 29208, Senior Member AIAA
† Graduate Assistant and PhD Candidate, Department of Mechanical Engineering, Univ. of South Carolina, 300 S. Main St., Columbia, SC 29208
‡ USAF, Air Force Research Lab, Materials and Manufacturing Directorate, AFRL/MLLP, 2230 Tenth Street, Wright-Patterson AFB, OH 45433

Report Documentation Page

Form Approved
OMB No. 0704-0188

1. REPORT DATE	2. REPORT TYPE	3. DATES COVERED
2004	**N/A**	**-**

4. TITLE AND SUBTITLE	5a. CONTRACT NUMBER
Embedded Ultrasonic Structural Radar with Piezoelectric Wafer Active Sensors for Damage Detection in Cylindrical Shell Structures	5b. GRANT NUMBER
	5c. PROGRAM ELEMENT NUMBER
6. AUTHOR(S)	5d. PROJECT NUMBER
	5e. TASK NUMBER
	5f. WORK UNIT NUMBER
7. PERFORMING ORGANIZATION NAME(S) AND ADDRESS(ES) **University of South Carolina, Department of Mechanical Engineering, Columbia, SC 29208**	8. PERFORMING ORGANIZATION REPORT NUMBER
9. SPONSORING/MONITORING AGENCY NAME(S) AND ADDRESS(ES)	10. SPONSOR/MONITOR'S ACRONYM(S)
	11. SPONSOR/MONITOR'S REPORT NUMBER(S)

12. DISTRIBUTION/AVAILABILITY STATEMENT
Approved for public release, distribution unlimited

13. SUPPLEMENTARY NOTES
The original document contains color images.

14. ABSTRACT

15. SUBJECT TERMS

16. SECURITY CLASSIFICATION OF:			17. LIMITATION OF ABSTRACT	18. NUMBER OF PAGES	19a. NAME OF RESPONSIBLE PERSON
a. REPORT	b. ABSTRACT	c. THIS PAGE			
unclassified	**unclassified**	**unclassified**	**UU**	**14**	

and comb transducers) are relatively too heavy and expensive to consider for widespread deployment on an aircraft structure as part of a SHM system. Hence, a different type of sensors than the conventional ultrasonic transducers is required for the SHM systems. Piezoelectric wafer active sensors (PWAS) are inexpensive, non-intrusive, un-obtrusive devices that can be used in both active and passive modes. In active mode, PWAS generated Lamb waves that can be used for damage detection through pulse-echo or pitch-catch techniques.

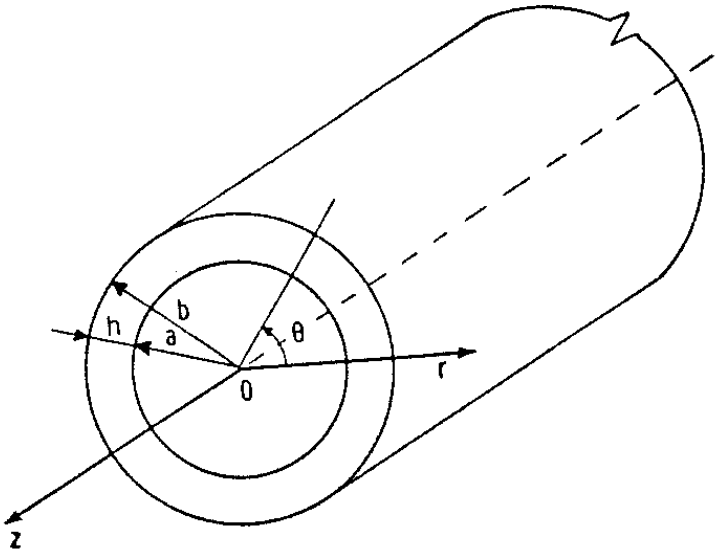

Figure 1 Reference coordinates and characteristic dimensions of a hollow cylinder in which guided waves are propagated (after ref. 10)

II. Guided Waves in Thin-wall Cylindrical Shells

In flat plates, ultrasonic guided waves travel as Lamb waves and as shear horizontal (SH) waves. Lamb waves are vertically polarized, while SH waves are horizontally polarized. Lamb waves can be symmetrical or antisymmetrical with respect to the plate midplane. At lower frequency-thickness products, only two Lamb wave types exist: S_0, which is a symmetrical Lamb wave type resembling the longitudinal waves; and A_0, which is an antisymmetric Lamb wave type resembling the flexural waves. At higher frequency-thickness values, a number of Lamb waves are present, S_n and A_n, where n = 0, 1, 2, … At very high frequencies, the S_0 and A_0 Lamb waves coalesce into the Rayleigh waves, which are confined to the plate upper and lower surfaces. The Lamb waves are highly dispersive (wave speed varies with frequency); however, S_0 waves at low frequency-thickness values show very little dispersion. The SH waves are also dispersive, with the exception of the first mode, SH_0, which does not show any dispersion at all. Ultrasonic guided waves in flat plates were first described by Lamb[1]. A comprehensive analysis of Lamb wave was given by Viktorov[2], Achenbach[3], Graff[4], Rose[5], and Royer & Dieulesaint[6].

The guided Lamb waves have the important property that they stay confined inside the walls of a thin-wall structure, and hence can travel over large distances. In addition, the guided waves can also travel inside curved walls; this property makes them ideal for applications in the ultrasonic inspection of aircraft, missiles, pressure vessel, oil tanks, pipelines, etc. The study of guided waves propagation in cylindrical shells can be considered a limiting case of the study of guided waves propagation in hollow cylinders. As the wall thickness of the hollow cylinder decrease with respect to its radius, the hollow cylinder approaches the case of a thin-wall cylindrical shell. Several investigators have considered the propagation of waves in solid and hollow cylinders. Love[7] studied wave propagation in an isotropic solid cylinder and showed that three types of solutions are possible: (1) longitudinal; (2) flexural; and (3) torsional. At high frequencies, each of these solutions is multimodal and dispersive. Meitzler[8] showed that, under certain conditions, mode coupling can exist between the various wave types propagating in solid cylinders such as wires. Extensive numerical simulation and experimental testing of these phenomena was done by Zemenek[9].

Comprehensive work on wave propagation in hollow circular cylinders was done by Gazis[10]. A comprehensive analytical investigation was complemented by numerical studies. The nonlinear algebraic equations and the

corresponding numerical solutions of the wave-speed dispersion curves were obtained. These results work found important applications in the ultrasonic nondestructive evaluation (NDE) of tubing and pipes. Silk and Bainton[11] found equivalences between the ultrasonic in hollow cylinders and the Lamb waves in flat plates and used them to detect cracks in heat exchanger tubing. Rose et al.[12] used guided pipe waves to find cracks in nuclear steam generator tubing. Alleyne et. al.[13] used guided waves to detect cracks and corrosion in chemical plant pipework.

A brief review of the mathematical modeling and the main results for guided waves in cylindrical shells are given next[10,11, 12]. The coordinates and characteristic dimensions are shown in Figure 1; *a* and *b* are the inner and outer radii of the tube, and *h* is the tube thickness. The variables *r, θ*, and *z* are the radial, circumferential, and longitudinal coordinates. The modeling starts from the equation of motion for an isotropic elastic medium, in invariant form:

$$\mu\Delta\mathbf{u} + (\lambda+\mu)\nabla\nabla\bullet\mathbf{u} = \rho(\partial^2\mathbf{u}/\partial t^2) \tag{1}$$

where **u** is the displacement vector, ρ is the density, λ and μ are Lame's constants, and Δ is the three-dimensional Laplace operator. The vector **u** is expressed in terms of the dilation scalar potential ϕ and the equivolume vector potential **H** according to:

$$\mathbf{u} = \nabla\phi + \nabla\times\mathbf{H} \tag{2}$$

$$\nabla\bullet\mathbf{H} = F(\mathbf{r},t) \tag{3}$$

For free motion, the displacement equations of motion are satisfied if the potentials ϕ and **H** satisfy the wave equations

$$c_P^2\Delta\phi = \partial^2\phi/\partial t^2 \tag{4}$$

$$c_S^2\Delta\mathbf{H} = \partial^2\mathbf{H}/\partial t^2 \tag{5}$$

where $c_P^2 = (\lambda+2\mu)/\rho$ and $c_S^2 = \mu/\rho$ are the pressure and shear wave speeds, respectively. We express the potentials and the wave equations in cylindrical coordinates as

$$\begin{aligned}
\phi &= f(r)\cos n\theta\cos(\omega t+\xi z)\\
H_r &= g_r(r)\sin n\theta\sin(\omega t+\xi z)\\
H_\theta &= g_\theta(r)\cos n\theta\sin(\omega t+\xi z)\\
H_z &= g_z(r)\sin n\theta\cos(\omega t+\xi z)
\end{aligned} \tag{6}$$

where wave motion along the *z* axis with wave number ξ is assumed. Substitution of Equation (6) into Equations (4) and (5) yields

$$\begin{aligned}
&(\Delta+\omega^2/c_P^2)\phi = 0\\
&(\Delta+\omega^2/c_S^2)H_z = 0\\
&(\Delta-1/r^2+\omega^2/c_S^2)H_r - (2/r^2)(\partial H_\theta/\partial\theta) = 0\\
&(\Delta-1/r^2+\omega^2/c_S^2)H_\theta + (2/r^2)(\partial H_r/\partial\theta) = 0
\end{aligned} \tag{7}$$

where $\Delta = \nabla^2$ is the Laplace operator. The following notations are introduced:

$$\alpha^2 = \omega^2/c_P^2 - \xi^2, \quad \beta^2 = \omega^2/c_S^2 - \xi^2 \tag{8}$$

The general solution is expressed in terms of Bessel functions *J* and *Y* or the modified Bessel functions *I* and *K* of arguments $\alpha_1 r = |\alpha r|$ and $\beta_1 r = |\beta r|$ as determined by Equation (8) are real or imaginary. The general solution is of the form

$$\begin{aligned}
f &= A\cdot Z_n(\alpha_1 r) + B\cdot W_n(\alpha_1 r)\\
g_3 &= A_3\cdot Z_n(\beta_1 r) + B_3\cdot W_n(\beta_1 r)\\
g_1 &= \tfrac{1}{2}(g_r - g_\theta) = A_1\cdot Z_{n+1}(\beta_1 r) + B_1\cdot W_{n+1}(\beta_1 r)\\
g_2 &= \tfrac{1}{2}(g_r + g_\theta) = A_2\cdot Z_{n-1}(\beta_1 r) + B_2\cdot W_{n-1}(\beta_1 r)
\end{aligned} \tag{9}$$

where, for brevity, *Z* denotes a *J* or *I* Bessel function, and *W* denotes a *Y* or a *K* Bessel function, as appropriate. Thus, the potentials are expressed in terms of the unknowns *A, B, A_1, B_1, A_2, B_2, A_3, B_3*. Two of these unknowns are eliminating using the gauge invariance property of the equivolume potentials. The strain-displacement and stress-strain relations are used to express the stresses in terms of the potential functions. Then, we impose the free-motion boundary conditions

$$\sigma_{rr} = \sigma_{rz} = \sigma_{r\theta} = 0 \quad \text{at} \quad r = a \quad \text{and} \quad r = b \tag{10}$$

Thus, one arrives at a linear system of six homogeneous equations in six unknowns. For nontrivial solution, the system determinant must vanish, i.e.,

$$\left|c_{ij}\right| = 0 \text{ , } i,j = 1 \ldots 6 \qquad (11)$$

The coefficients c_{ij} in Equation (11) have complicated algebraic expressions (Gazis, 1959) that are not reproduced here for sake of brevity. We retain, however, that a characteristic equation exists in the form:

$$\Omega_n(a,b,\lambda,\mu,fd,c) = 0 \qquad (12)$$

where a and b represent the inner and outer radii of the tube, while λ and μ represent the Lame constants. This implicit transcendental equation is solved numerically to determine the permissible guided-wave solutions. As shown by Gazis[10], three basic families of guided waves exist:

- Longitudinal axially symmetric modes, L(0, m), m = 1, 2, 3, …
- Torsional axially symmetric modes, T(0, m) , m = 1, 2, 3, …
- Flexural non-axially symmetric modes, F(n, m), n = 1, 2, 3, … m = 1, 2, 3, …

Within each family, an infinite number of modes exist such that their phase velocities, c, for a given frequency-thickness product, fd, represent permissible solutions of an implicit transcendental Equation (12). The index m represents the number of the mode shape across the wall of the tube. The index n determines the manner in which the fields generated by the guided wave modes vary with angular coordinate θ in the cross-section of the cylinder. For the F modes of family n, each field component can be considered to vary as either $\sin(n\theta)$ or $\cos(n\theta)$. It is also observed that the index n represents the mode shape of flexing of the tube as a whole.

The longitudinal and torsional modes are also referred to as the axial symmetric or n = 0 modes. These axial symmetric modes are preferred for defect detection in long pipes since the pipe circumference is uniformly insonified. The longitudinal modes are easier to generate with conventional ultrasonic transducers. They are good for the location of circumferential cracks. However, for the location of axial cracks and corrosion, the torsional modes, though more difficult to generate with conventional ultrasonic transducers, are recommended.

Thus, the existence in thin-wall cylinders of guided waves similar to the Lamb waves present in flat plates was identified. An examination of the differential equations dependence on the ratios h/r and h/λ indicates that, for shallow shells (h/r and $h/\lambda << 1$), the longitudinal modes approach the Lamb wave modes, whereas the torsional modes approach the SH modes. In fact, it can be shown that the L(0,1) mode corresponds to the A_0 Lamb mode, while the L(0,2) mode corresponds to the S_0 Lamb mode, etc. The flexural modes remain a mode type specific to tube waves and without equivalence in flat plate waves.

(a) 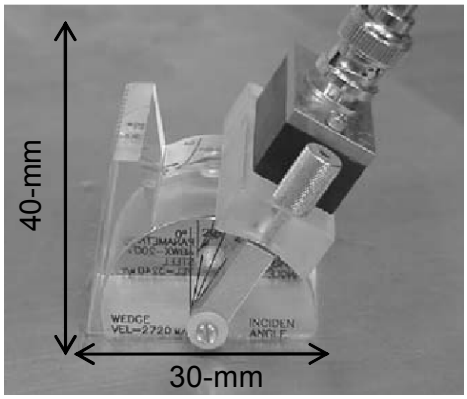

(b) 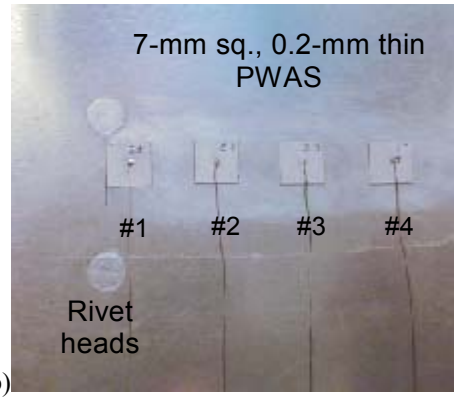

Figure 2: (a) conventional Lamb wave ultrasonic transducer (~25 grams, ~$400, 40-mm tall); (b) piezoelectric wafer active sensors (PWAS): 0.08 grams, $15, 0.2 mm thin.

III. Guided-Wave Generation/Detection with Piezoelectric Wafer Active Sensors

In conventional ultrasonics, guided waves are generated by impinging the structural surface obliquely with a ultrasonic beam from a relatively large ultrasonic transducer affixed to a wedge. Snell's law ensures mode conversion at the interface, hence a combination of pressure and shear waves are simultaneously generated into the structure. If the structure is thin walled, guided plate of shell waves are being created. Another method of creating guided waves in a structure is by using a comb transducer. The comb spacing is such that it tunes with the guided wave half wavelength. However, conventional Lamb-wave probes (wedge and comb transducers) are relatively too heavy and expensive to be considered for widespread deployment on an aircraft structure as part of a SHM system. A typical wedge transducer weighs 25 grams, costs ~$400, and is 40-mm tall (Figure 2a). Hence, a different type of sensors than the conventional ultrasonic transducers is required for the SHM systems.

In recent years, piezoelectric wafers permanently attached to the structure have been extensively used for the generation and detection of guided waves. These simple devices are inexpensive, very lightweight, and unobtrusive (Figure 2b). They seem ideally suited for structural health monitoring applications. They can act as both transmitters and receivers of ultrasonic waves. They are called *piezoelectric wafer active sensors* (PWAS). PWAS weight around 68 mg, are 0.2 mm thick, and cost only ~$15 each.

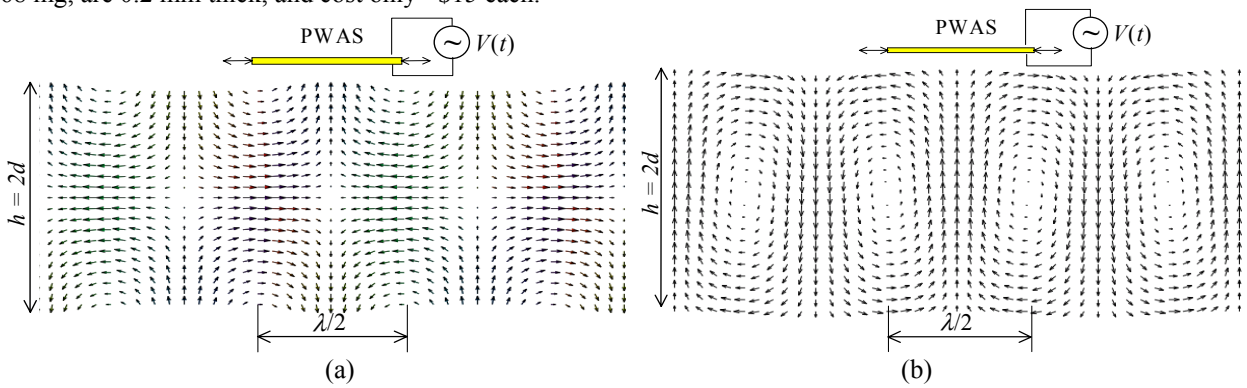

Figure 3 PWAS interaction with S_0 and A_0 Lamb modes

PWAS operated on the piezoelectric principle that couples the electrical and mechanical variables in the material (mechanical strain, S_{ij}, mechanical stress, T_{kl}, electrical field, E_k, and electrical displacement D_j) in the form:

$$\begin{aligned} S_{ij} &= s^E_{ijkl} T_{kl} + d_{kij} E_k \\ D_j &= d_{jkl} T_{kl} + \varepsilon^T_{jk} E_k \ , \end{aligned} \tag{13}$$

where s^E_{ijkl} is the mechanical compliance of the material measured at zero electric field ($E = 0$), ε^T_{jk} is the dielectric permittivity measured at zero mechanical stress ($T = 0$), and d_{kij} represents the piezoelectric coupling effect. For embedded NDE applications, PWAS couple their in-plane motion, excited by the applied oscillatory voltage through the piezoelectric effect, with the Lamb-waves particle motion on the material surface. Lamb waves can be either quasi-axial (S0, S1, S2, …), or quasi-flexural (A0, A1, A2, …) as shown in Figure 3. PWAS transducers can act as both exciters and detectors of the elastic Lamb waves traveling in the material. PWAS can be used as both active and passive probes and thus can address **four SHM** needs:

1. **Active sensing of far-field damage** using pulse-echo, pitch-catch, and phased-array methods
2. **Active sensing of near-field damage** using high-frequency impedance method
3. **Passive sensing of crack initiation and growth** through acoustic emission
4. **Passive sensing of damage-generating events** through detection of low-velocity impacts

An important characteristic of PWAS, which distinguishes them from conventional ultrasonic transducers, is their capability of tuning into various guided wave modes. Though a complete modeling of this interaction is not yet available, some simplified models exist that clarify the underlying principles. Giurgiutiu[14] developed a 1-D analysis of the PWAS-structure interaction using the space-domain Fourier analysis. This model illustrates the principles of PWAS Lamb-wave mode tuning, and opens the path for a more comprehensive analysis. The analysis starts with transformed equations:

$$\frac{d^2\tilde{\phi}}{dy^2}+p^2\tilde{\phi}=0\,,\qquad \frac{d^2\tilde{\psi}}{dy^2}+q^2\tilde{\psi}=0\qquad p^2=\frac{\omega^2}{c_L^2}-\xi^2\,,\qquad q^2=\frac{\omega^2}{c_T^2}-\xi^2 \tag{14}$$

where $\tilde{\phi}$ and $\tilde{\psi}$ are the transformed potential functions, $c_L^2=(\lambda+2\mu)/\rho$ and $c_T^2=\mu/\rho$ are the longitudinal (pressure) and transverse (shear) wave speeds, λ and μ are Lame constants, ρ is the mass density. The excitation is assumed in the form of time-harmonic shear stress, $\tau_a(x)e^{-i\omega t}$, applied by the PWAS to the structural surface over the interval $-a < x < +a$. Assuming perfect bonding between PWAS and structure concentrates the shear transfer effects at the PWAS ends. Hence, the shear stress $\tau(x)$ and its Fourier transform $\tilde{\tau}(\xi)$ are given by

$$\tau(x)=a\tau_0\left[\delta(x-a)-\delta(x+a)\right],\quad \tilde{\tau}(\xi)=a\tau_0\left[-2i\sin\xi a\right] \tag{15}$$

where $\delta(x)$ is the Dirac function. Equations (14), (15) accept the Fourier-domain solution:

$$\tilde{\varepsilon}_x=-i\frac{\tilde{\tau}}{2\mu}\left(\frac{N_S}{D_S}+\frac{N_A}{D_A}\right),\qquad \tilde{u}_x=-i\frac{\tilde{\tau}}{2\mu}\frac{1}{\xi}\left(\frac{N_S}{D_S}+\frac{N_A}{D_A}\right) \tag{16}$$

where $\tilde{\varepsilon}_x$ is the axial strain, $\tilde{u}_x$ is the axial displacement, and

$$\begin{aligned} N_S&=\xi q(\xi^2+q^2)\cos ph\cos qh,\quad D_S=(\xi^2-q^2)^2\cos ph\sin qh+4\xi^2 pq\sin ph\cos qh\\ N_A&=\xi q(\xi^2+q^2)\sin ph\sin qh,\quad D_A=(\xi^2-q^2)^2\sin ph\cos qh+4\xi^2 pq\cos ph\sin qh \end{aligned} \tag{17}$$

Applying the inverse Fourier transform in the space domain, and adding the time-domain harmonic behavior yields the forward wave solution:

$$\varepsilon_x(x,t)=\frac{1}{2\pi}\frac{-i}{2\mu}\int_{-\infty}^{\infty}\left(\frac{\tilde{\tau}N_S}{D_S}+\frac{\tilde{\tau}N_A}{D_A}\right)e^{i(\xi x-\omega t)}d\xi\qquad u_x(x,t)=\frac{1}{2\pi}\frac{-i}{2\mu}\int_{-\infty}^{\infty}\frac{1}{\xi}\left(\frac{\tilde{\tau}N_S}{D_S}+\frac{\tilde{\tau}N_A}{D_A}\right)e^{i(\xi x-\omega t)}d\xi \tag{18}$$

The integral in Equation (18) is singular at the roots of D_S and D_A. These roots correspond to the symmetric and anti-symmetric Lamb wave modes having eigenvalues, $\xi_0^S,\xi_1^S,\xi_2^S,\ldots\ \xi_0^A,\xi_1^A,\xi_2^A,\ldots$ The integral in Equation (18) is evaluated through the residue theorem, using a semicircular contour consisting in the upper half of the complex ξ plane. Hence,

$$\varepsilon_x(x,t)=-i\frac{a\tau_0}{\mu}\sum_{\xi^S}\sin\xi^S a\frac{N_S(\xi^S)}{D_S'(\xi^S)}e^{i(\xi^S x-\omega t)}-i\frac{a\tau_0}{\mu}\sum_{\xi^A}\sin\xi^A a\frac{N_A(\xi^A)}{D_A'(\xi^A)}e^{i(\xi^A x-\omega t)} \tag{19}$$

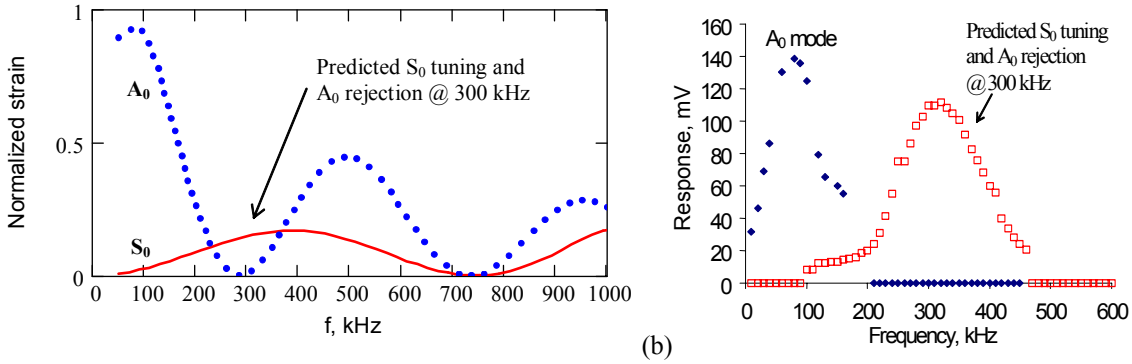

Figure 4 (a) Predicted Lamb wave strain amplitude in a 1-mm aluminum plate under a 7-mm PWAS excitation; (b) experimental verification of excitation sweet spot at 300 kHz (ref. 14)

The summations in Equations (19) cover all the symmetric (ξ^S) and anti-symmetric (ξ^A) Lamb wave modes that exist for a given value of ω in a given plate[14]. A plot of this solution in the 0–1000 kHz bandwidth is presented in Figure 4a. **The $\sin\xi a$ contained in Equation (19) displays maxima when the PWAS length l_a = 2a equals an odd multiple of the half wavelength, and minima when it equals an even multiple of the half wavelength.** Several such maxima and minima exist, each associated with a certain Lamb mode of its own wavelength. These minima and maxima allows us to achieve Lamb-mode tuning. We can tune into a selected Lamb mode by choosing the appropriate frequency and PWAS geometry. Figure 4a illustrates the tuning of the S_0 mode at 300 kHz. This happens because at this frequency, the amplitude of the A_0 mode goes through zero while that of the S_0 is still strong. Thus,

we have **tuning of the S_0 mode, and rejection of the A_0 mode**. Figure 4b shows the experimental confirmation of this S_0 "sweet spot". Lamb wave mode tuning offers considerable advantages. It allows us to select Lamb wave modes that are most appropriate for the particular application being considered. The tuning of the S_0 mode is important for the detection of certain defects, such as cracks. The S_0 mode is less dispersive than the A_0 mode at low *fd* values and produces better wave packets. When the A_0 mode is rejected, the remaining S_0 mode gives loud and clear pulse-echo reflections from the through-the-thickness cracks[15].

IV. Phase Array Principles Used in the Embedded Ultrasonic Structural Radar

An important application of the PWAS based ultrasonics is that based on phased array principles. Giurgiutiu and Bao[16] developed a PWAS phased array application and named it embedded ultrasonics structural radar (EUSR). Its principle of operation is derived from two general concepts:

(1) The of guided Lamb wave generation with piezoelectric wafer active sensors (PWAS)
(2) The principles of conventional phased-array radar.

The phased array beam forming principles can be easily understood through the following 3-element array example presented in Figure 5. In this example, three wave sources were placed half wave length apart. When activated, the waves generated by each source would interfere in the wave field, generating constructive and destructive interference patterns. The beam in the middle corresponds to where the constructive interference is at a maximum. By timing the relative phase between the wave signals emanating from each source, the beam of maximum constructive interference can be steered around the horizon.

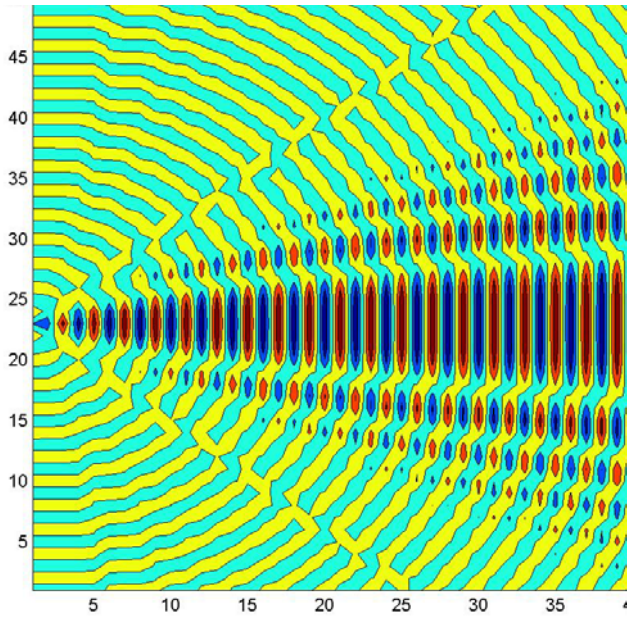

Figure 5 Simulated beam forming from a 3-element array

Lamb waves can exist in a number of dispersive modes. However, through smoothed tone-burst excitation and frequency tuning, it is possible to confine the excitation to a particular Lamb wave mode, of carrier frequency f_c, wave speed c, and wave length $\lambda = c/f_c$. Hence, the smoothed tone-burst signal generated by one PWAS is of the form:

$$s_T(t) = s_0(t)\cos 2\pi f_c t \tag{20}$$

where $s_0(t)$ is a short-duration smoothing window that is applied to the carrier signal of frequency f_c between 0 and t_p.

The principles of conventional phased-array radar[17] are applied to the PWAS array, assuming a uniform linear array of M PWAS, with each PWAS acting as a point-wise omni-directional transmitter and receiver. The PWAS in the array are spaced at the distance d, which is assumed much smaller than the distance r to a generic, far-distance point, P. Since d << r, the rays joining the sensors with the point P can be assimilated with a parallel fascicle, of ϕ. Therefore, for the m^{th} PWAS, the distance will be shorted by $m(d\cos\phi)$. If all the PWAS are fired simultaneously, the signal from the m^{th} PWAS will arrive at P quicker by $\Delta_m(\phi) = m(d\cos\phi)/c$. Yet, if the PWAS are not fired simultaneously, but with some individual delays, δ_m, m = 0,1,…,M-1, then the total signal received at point P will be:

$$s_{\mathrm{P}}(t) = \frac{1}{\sqrt{r}}\sum_{m=0}^{M-1} s_{\mathrm{T}}\left(t - \frac{r}{c} + \Delta_m(\phi) - \delta_m\right) \tag{21}$$

where $1/r$ represents the decrease in the wave amplitude due to the omni-directional 2-D radiation, and r/c is the delay due to the travel distance between the reference PWAS (m = 0) and the point P. (Here wave-energy conservation, i.e., no dissipation, is assumed.)

Transmitter beamforming: if we have $\delta_m = m\Delta(\phi)$, then Equation (21) becomes:

$$s_{\mathrm{P}}(t) = M \cdot \frac{1}{\sqrt{r}} s_{\mathrm{T}}\left(t - \frac{r}{c}\right) \tag{22}$$

That's to say, there is an M times increase in the signal strength with respect to a simple sensor. This leads directly to the beamforming principle that if $\delta_m = md\cos(\phi_0)/c$, and since $\Delta_m = md\cos(\phi)/c$, then constructive interference (beamforming) takes place when $\cos(\phi) = \cos(\phi_0)$, i.e. at angles $\phi = \phi_0$ and $\phi = -\phi_0$. Thus, the forming of a beam at angles ϕ_0 and $-\phi_0$ is achieved through delays in the firing of the sensors in the array.

Receiver beamforming: if the point P is an omni-directional source at azimuth ϕ_0, then the signals received at the m$^{\mathrm{th}}$ sensor will arrive quicker by $m\Delta_0\phi = md\cos(\phi_0)/c$. Hence, we can synchronize the signals received at all the sensors by delaying them by:

$$\delta_m(\phi_0) = m\frac{d}{c}\cos(\phi_0) \tag{23}$$

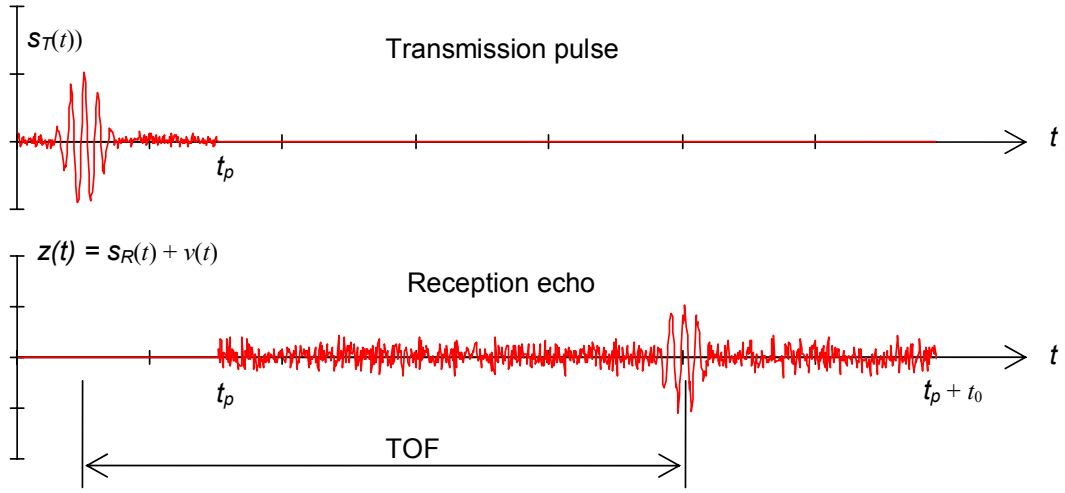

Figure 6 The basis of pulse-echo method: (a) transmitted smooth-windowed tone-burst of duration t_p; (b) received signal to be analyzed for the duration t_0, starting at t_p, in order to identify the time of flight delay, τ.

Pulse-echo method: Assume that a target exists at azimuth ϕ_0 and distance R. The transmitter beamformer is sweeping the range in increasing angles ϕ and receives an echo when $\phi = \phi_0$. The echo will be received on all sensors, but the signals will not be synchronized. To synchronize the sensors signals, the delays $\delta_m(\phi_0) = md\cos(\phi_0)/c$ need to be applied.
The original signal is:

$$s_{\mathrm{P}}(t) = \frac{M}{\sqrt{R}} s_{\mathrm{T}}\left(t - \frac{2R}{c}\right) \tag{24}$$

At the target, the signal is backscattered with a backscatter coefficient, A. Hence, the signal received at each sensor will be:

$$\frac{A \cdot M}{R} s_{\mathrm{T}}\left(t - \frac{2R}{c} + \Delta_m(\phi)\right) \tag{25}$$

The receiver beamformer assembles the signals from all the sensors with the appropriate time delays:

$$s_{\mathrm{R}}(t) = \frac{A \cdot M}{R} \sum_{m=0}^{M-1} s_{\mathrm{T}}\left(t - \frac{2R}{c} + \Delta_m(\phi) - \delta_m\right) \tag{26}$$

Constructive interference between the received signals is achieved when $\delta_m = md\cos(\phi_0)/c$. Thus, the assembled receive signal will be again boosted M times, with respect to the individual sensors:

$$s_R(t) = \frac{A \cdot M^2}{R} \sum_{m=0}^{M-1} s_T\left(t - \frac{2R}{c}\right) \tag{27}$$

Then the target range can be calculated as:

$$R = c\tau / 2 \tag{28}$$

Therefore, what we need to determine from the signals is the time delay between the receive signal, $s_R(t)$ and the transmit signal $s_T(t)$. Figure 6 shows the transmitted and received signals.

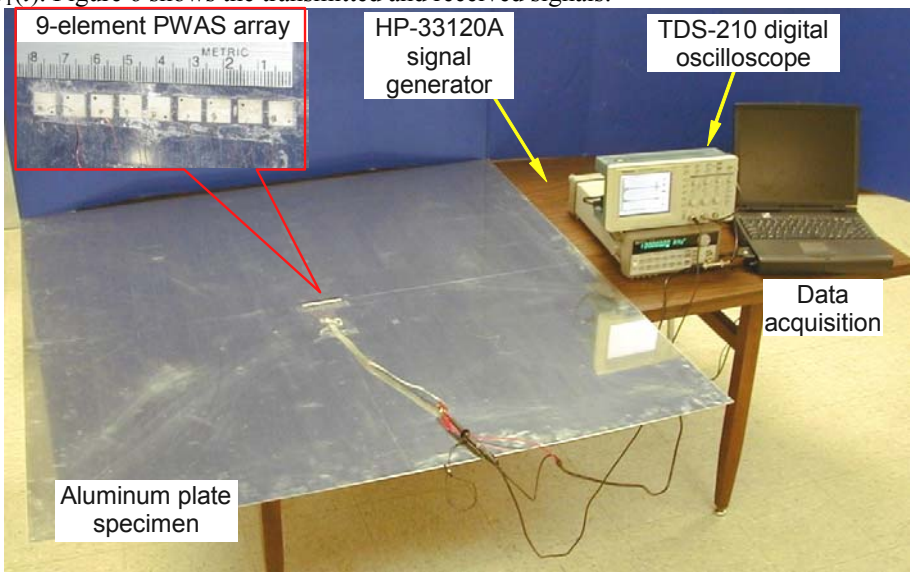

Figure 7 Experimental setup for the EUSR experiment

V. Experimental Results

To verify the theoretical results, experiments were conducted at the University of South Carolina in the Laboratory for Adaptive Materials and Smart Structures (LAMSS). The experimental setup is presented in Figure 7. The experimental setup has been identical with that used previously in the development of the EUSR concept on a flat plate. It consists of a 1-mm thick aluminum plate of square geometry (1220 mm by 1200 mm). A PWAS array was constructed in the middle of the plate. The PWAS array consisted of nine piezoelectric wafers (APC 850 piezoceramic, 0.2 mm thick, 7 mm by 7 mm square). The PWAS array was wired to a connection pad. An HP-33120A signal generator was used to produced a 3-count smoothed tone burst of 300 kHz. The excitation frequency was such as to tune into the S0 Lamb wave mode. A TDS-210 digital oscilloscope was used to collect and digitize the signals. The signal generation and collection proceeded in a round-robin fashion. In turns, one PWAS was transmitter and all the other PWAS were receiver. The signal was collected on all the receivers and also on the transmitter. Then, the next PWAS in the array became transmitter and the process repeated. Thus, a total of $9 \times 9 = 81$ elemental signals were collected. These signals were processed with the EUSR algorithm. Figure 8a shows the location and size of the simulated crack (narrow slit). Figure 8b shows the imaging of the crack on the EUSR GUI and the reconstructed pulse-echo signal (A scan). The signal reconstruction and the crack imaging were done in virtual time by applying the EUSR algorithm to the set of 81 elemental signals. Figure 8b shows the A scan of the crack echo recorded as the virtual beam points to an azimuth angle of 90^0. Loud and clear reception of the echo signal is observed. During interactive tests, it was found that this echo diminishes rapidly as the beam direction shifts to the right and to the left of the simulated crack target. By stepping the scanning beam through the interval 0^0 to 180^0, a complete scan of the plate upper half could be obtained. Putting together all these beams in a polar plot, and using a color scale of the signal amplitude we were able to create a mapped image of the plate upper half. In this mapped image, the crack location is clearly defined by a pronounced color change (Figure 8b).

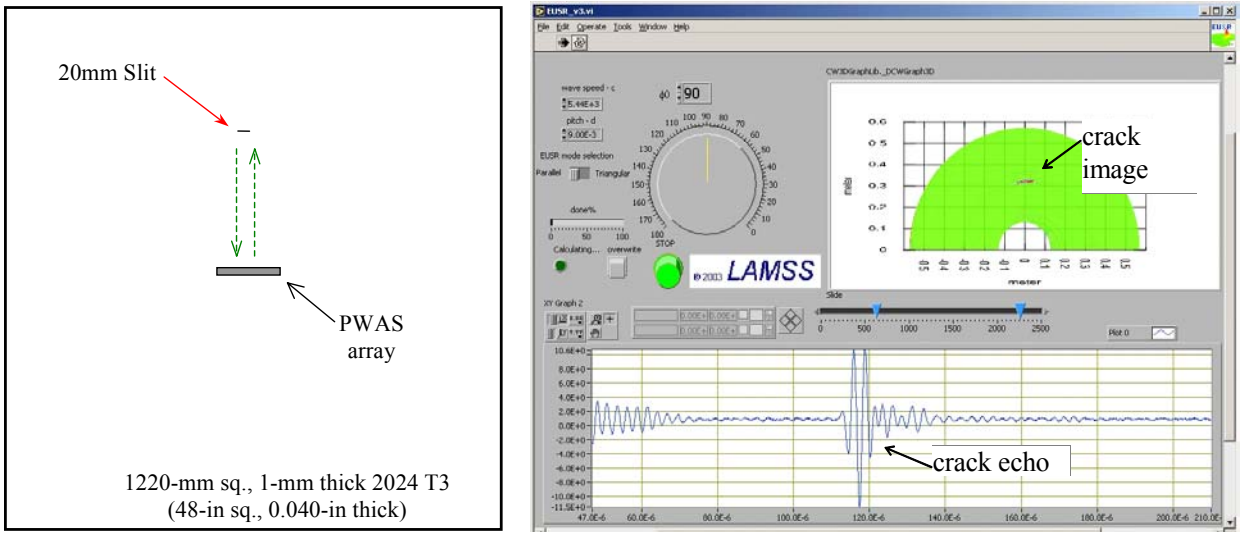

(a) (b)

Figure 8 Crack detection at zero curvature (flat plate): (a) location and size of simulated crack; (b) crack imaging and crack echo in the EUSR algorithm

Table 1 Curvature of the specimen

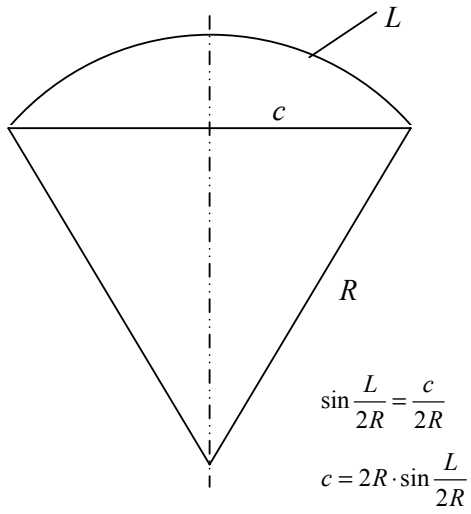

$$\sin\frac{L}{2R}=\frac{c}{2R}$$

$$c=2R\cdot\sin\frac{L}{2R}$$

R	c	ΔL=L-c
100.00E+3	1219.99	
50.00E+3	1219.97	
20.00E+3	1219.81	
10.00E+3	1219.24	
8.80E+3	1219.02	1
5.00E+3	1216.98	
3.90E+3	1215.03	5
2.75E+3	1210.02	10
2.24E+3	1204.98	15
2.00E+3	1201.17	
1.95E+3	1200.20	20
1.00E+3	1145.73	

L = 1220, all in mm

In order to verify the effect of curvature, the thin aluminum plate was temporary bent into cylindrical shapes using thin wire ropes and tightening screws. The realized curvatures were related to the shortening of the chord with respect to the original flat length. After curving, the original flat length, L, became the circular arc, while the shorted wire rope became the chord, c. The difference between the original length, L, and the shortened length, c, was denoted by ΔL. The chord c can be calculated with the formula

$$c=2R\sin\frac{L}{2R} \tag{29}$$

Then, the radius of curvature, R, could be calculated with the formula:

$$R=\frac{L-\Delta L}{2\sin\frac{L}{2R}} \tag{30}$$

The values of curvature obtained with Equation (30) are given in Table 1. In our experiment we went through the shortenings ΔL = 5mm, 10mm, 15mm and 20mm corresponding to curvature values R = 3.90 m, 2.75 m, 2.24 m, 1.95 m. These curvatures were applied in two directions. One direction was with the chord parallel to the PWAS array (direction 1), while the other was with the chord perpendicular to the PWAS array (direction 2).

(a)

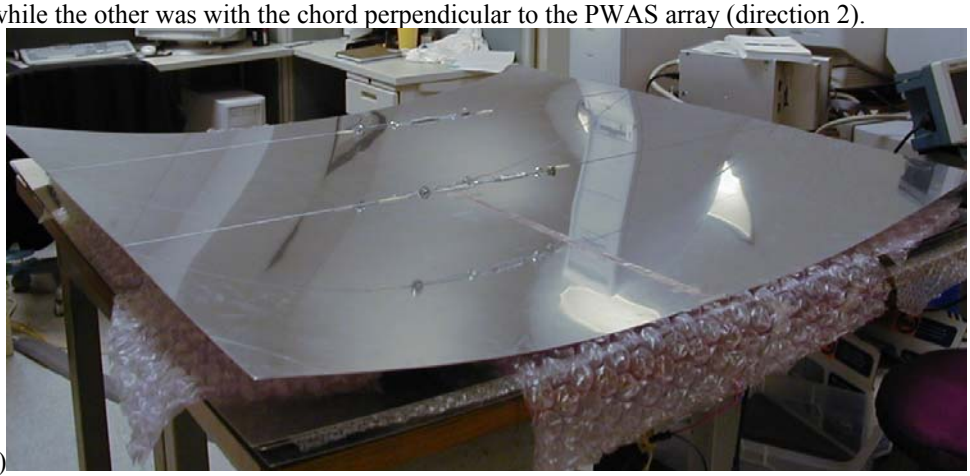

(b)

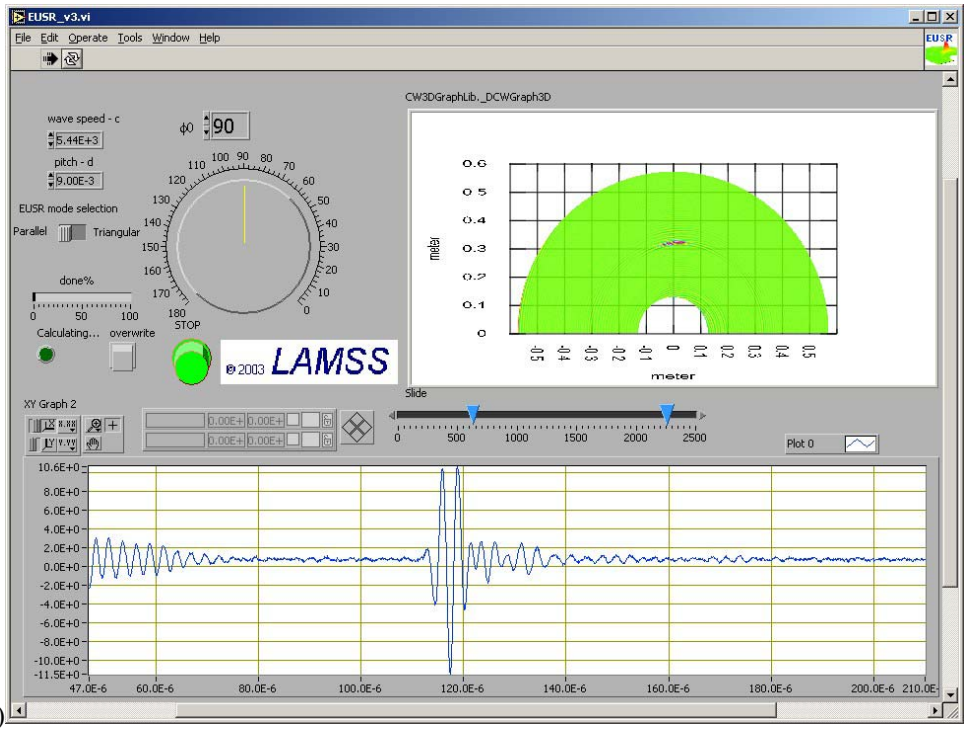

Figure 9 Crack detection at high curvature (R = 1.95 m) in direction 1: (a) photo of specimen while being bend; (b) crack imaging and crack echo in the EUSR algorithm

VI. Summary and Conclusions

This paper has discussed the use of the embedded ultrasonics structural radar (EUSR) with piezoelectric wafer active sensors (PWAS) for damage detection in cylindrical shell structures. This work is in continuation of previous work of similar nature performed on flat plates. In Section I, a brief introduction highlighting the advantages of using guided waves for nondestructive evaluation (NDE) of thin-wall structures was presented. Also discussed was the

need for unobtrusive low-cost and light weight transducers to be used in embedded structural health monitoring (SHM) system. The PWAS transducers were identified as strong candidates for performing this function.

Section II discussed guided waves in thin-wall cylindrical shells. The mathematical model for the analysis of wave propagation in hollow cylinders was reviewed and its general solution was presented. It was shown that the general solution accepts three wave types: (i) longitudinal axially symmetric modes, L(0, *m*), $m = 1, 2, 3, \ldots$; (ii) torsional axially symmetric modes, T(0, *m*) , $m = 1, 2, 3, \ldots$; and (iii) flexural non-axially symmetric modes, F(*n*, *m*), $n = 1, 2, 3, \ldots$, $m = 1, 2, 3, \ldots$ An examination of the differential equations dependence on the ratios h/r and h/λ indicates that, for shallow shells (h/r and $h/\lambda << 1$), the longitudinal modes approach the Lamb wave modes, whereas the torsional modes approach the SH modes. In fact, it can be shown that the L(0,1) mode corresponds to the A_0 Lamb mode, while the L(0,2) mode corresponds to the S_0 Lamb mode, etc. The flexural modes remain a mode type specific to tube waves and without equivalence in flat plate waves.

(a)

(b)

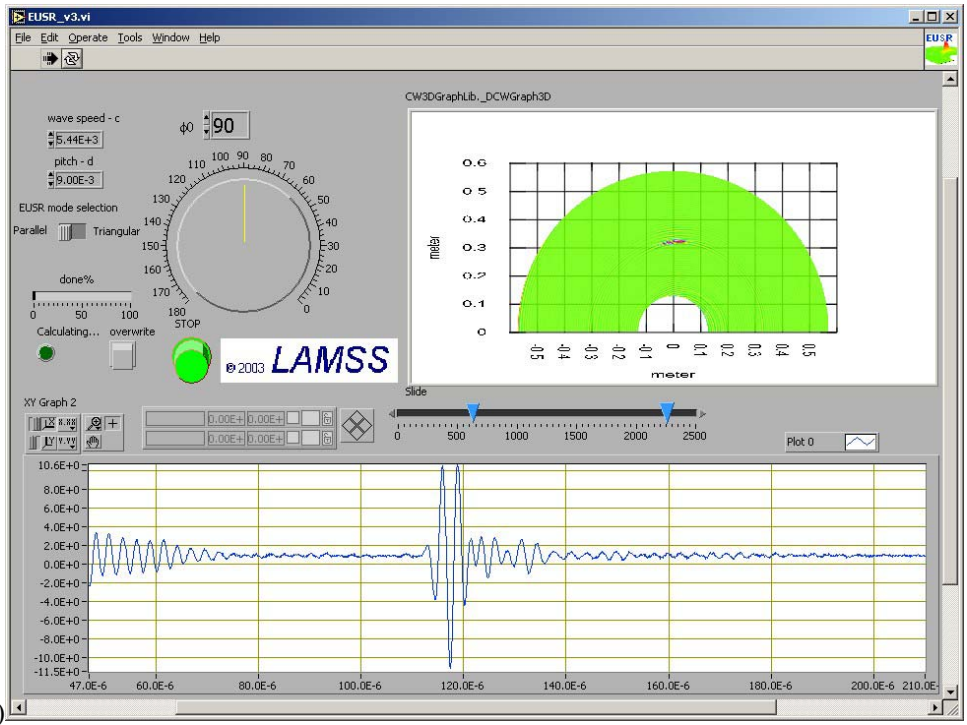

Figure 10 Crack detection at high curvature (R = 1.95 m) in direction 2: (a) photo of specimen while being bend; (b) crack imaging and crack echo in the EUSR algorithm

Section III discussed the guided-wave generation and detection with PWAS. It was shown that due to their bidirectional piezoelectric mechano-electrical coupling, PWAS can act as both generators and detectors of elastic

waves. PWAS can perform four SHM functions: (i) active sensing of far-field damage using pulse-echo, pitch-catch, and phased-array methods; (ii) active sensing of near-field damage using high-frequency impedance method; (iii) passive sensing of crack initiation and growth through acoustic emission; (iv) passive sensing of damage-generating events through detection of low-velocity impacts. The mathematical model of a PWAS mounted to the surface of a flat plate was presented. The general solution derived through the space-domain Fourier transform was reviewed. For the case of perfect bonding between the PWAS and the structure, a closed form solution was obtained. The closed-form solution is expressed as a summation of the individual responses of several Lamb wave modes. In this summation, the individual contribution of each Lamb wave mode varies with frequency. A plot of this solution vs. frequency indicated that Lamb wave tuning opportunities exist whereas, for a given PWAS geometry, certain frequencies exist that maximize the response of a particular Lamb wave mode with respect to the other modes. For a 1-mm thick aluminum plate, it was predicted that the high-dispersion A0 mode will be maximized at around 100 kHz while the low-dispersion S0 mode will be maximized at around 300 kHz. These theoretical predictions were verified very well by experimental results.

Section IV treated the phased array principles applied to arrays of PWAS. The discussion was started with the analysis of the wave field generated around three PWAS that were excited with a slight phase difference. It was shown that a ultrasonic beam can be formed through the constructive interference of the wave fields generated by the PWAS. The beam angle could be adjusted by changing the relative phase of the three elementary signals. These principles were extended to an array of M identical equally-spaced PWAS. Using the parallel-ray assumption, the transmission beamforming and reception beamforming algorithms were presented. Eventually, the formula for pulse-echo detection of defects using a scanning beam principle was derived. These principles were used to create the embedded ultrasonics structural radar (EUSR) algorithm with a graphical user interface (GUI) for virtual-time processing of phased-array signals.

In Section V, experimental results were presented. A 9-element PWAS array was constructed on a 1-mm thick 2024-T3 aluminum plate. A small narrow slit was manufactured in the plate to simulate crack damage. Using general purposes laboratory instrumentation, a set of 81 elemental signals was collected through round-robin excitation of the individual PWAS and collection of signals on all the PWAS. The signals corresponded to tuned excitation of the low-dispersion S0 Lamb wave mode. The elemental signals were processed in virtual time with the EUSR-GUI. Good and accurate imaging of the crack was obtained. Then, the effect of curvature on the crack detection capability was studied. Four curvature values were tested. The radius of curvature for these curvatures was 3.9 m (13 ft); 2.75 m (9.2 ft); 2.24 m (7.5 ft); 1.95 m (6.5 ft).The curvatures were applied in two directions: (1) with the chord parallel to the PWAS array; (2) with the chord perpendicular to the PWAS array. Good crack detection was obtained for all curvatures and all directions. No significant difference due to curvature could be observed.

We conclude that the EUSR method with PWAS phased arrays can be successfully applied to detect and image simulated cracks in cylindrical shell structures. Further work should focus on refining the theoretical and experimental results and then testing the method on realistic aerospace structures.

VII. Acknowledgments

Support from the Air Force Research Laboratory through UTC Contract #03-S470-033-C1 of F33615-01-D-5801 is thankfully acknowledged.

VIII. References

1. Lamb, H. (1917) “On Waves in an Elastic Plate”, *Proceedings of the Royal Society of London*, Series A, Vol. 93, 1917, pp. 114
2. Viktorov., I. A. (1967) *Rayleigh and Lamb Waves – Physical Theory and Applications*, Plenum Press, 1967
3. Achenbach, J. D. (1973) *Wave Propagation in Elastic Solids*, Elsevier, 1973
4. Graff, K. F. (1975) *Wave Motion in Solids*, Dover Publications, Inc., 1975
5. Rose, J. L. (1999) *Ultrasonic Waves in Solid Media,* Cambridge University Press, 1999
6. Royer, D.; Dieulesaint, E. (2000) *Elastic Waves in Solids*, Springer, 2000
7. Love, A. E. H. (1944) *A Treatise on the Mathematical Theory of Elasticity*, Dover Pub., NY, 1944
8. Meitzler, A. H. (1961) “Mode Coupling Occurring in the Propagation of Elastic Pulses in Wires”, *Journal of the Acoustical Society of America*, Vol. 33, No. 4, April 1961, pp. 435-445
9. Zemenek, J. (1972) “An Experimental and Theoretical Investigation of Elastic Wave Propagation in a Cylinder”, *Journal of the Acoustical Society of America*, Vol. 51, No, 1 (Part 2), 1972, pp. 265-283

10. Gazis, D. C. (1959) “Three Dimensional Investigation of the Propagation of Waves in Hollow Circular Cylinders”, *Journal of the Acoustical Society of America*, Vol. 31, No. 5, May 1959, pp. 568-578
11. Silk, M. G. ; Bainton, K. F. (1979) “The Propagation in Metal Tubing of Ultrasonic Wave Modes Equivalent to Lamb Waves”, *Ultrasonics*, Jan. 1979, pp. 11-19
12. Rose, J. L.; Ditri, J. J.; Pilarski, A.; Rajana, K.; Carr, F.T. (1994) “A Guided Wave Inspection Technique for Nuclear Steam Generator Tubing”, *NDT&E International*, Vol. 27, pp. 307-310, 1994
13. Alleyne, D.N., Pavlakovic, B., Lowe, M.J.S., Cawley, P. (2001) "Rapid, Long Range Inspection of Chemical Plant Pipework Using Guided Waves," *Review of Progress in QNDE*, Vol. 20, (2001), pp. 180-187
14. Giurgiutiu, V. (2003) “Lamb Wave Generation with Piezoelectric Wafer Active Sensors for Structural Health Monitoring”, *SPIE's 10th Annual International Symposium on Smart Structures and Materials and 8th Annual International Symposium on NDE for Health Monitoring and Diagnostics*, 2-6 March 2003, San Diego, CA, paper # 5056-17
15. Giurgiutiu, V.; Bao, J.; Zhao, W. (2003) “Piezoelectric-Wafer Active-Sensor Embedded Ultrasonics in Beams and Plates”, *Experimental Mechanics*, Sage Pub., Vol. 43, No. 4, December 2003, pp. 428-449
16. Giurgiutiu, V.; Bao, J. (2002) “Embedded Ultrasonic Structural Radar for the Nondestructive Evaluation of Thin-Wall Structures” Proceedings of the 2002 ASME International Mechanical Engineering Congress, November 17-22, 2002, New Orleans, LA, paper # IMECE2002-39017
17. Silvia, M. T. (1987) “*Time Delay Estimation*”, in *Handbook of Digital Signal Processing*, D. F. Elliot (Ed.), Academic Press, 1987